# Effects of three-dimensional external magnetic perturbations on prompt loss of fast ions from neutral beam injection on EAST tokamak

by Youjun Hu, Baolong Hao, Yongjian Xu, Yinfeng Xu

Institute of plasma physics, Chinese Academy of Sciences
Email: yjhu@ipp.cas.cn

**Abstract**

Axxxxx

## 1 Introduction

Heating tokamak plasma through injecting beams of energetic neutral particles is widely adopted in contemporary tokamak devices[?]. Since the injected particles are neutral, they are not influenced by the strong magnetic field of tokamaks, which makes it easy for them to enter the plasma. After entering the plasma, the neutral particles encouter collisions with ions and electrons of the background plasma, which makes them ionize and thus become fast ions. These fast ions then move under the influence of the strong magnetic field of tokamaks. The fast ions needs to stay within the plasma for a long time (of slowing-down time scale, $\sim$100ms for typical parameters of contemporary tokamak) to efficiently heat the thermal plasma through collision with the thermal ions and electrons. However, some fast ions are quickly lost to the wall of the device after thier birth becuase their orbits touch the wall. This kind of loss is usually called prompt loss or orbit loss. Whether a fast ions is lost or not depends on its velocity and birth location in the plasam. To estimate the fraction of fast ions that are prompt lost for a specific neutral beam injection (NBI) and a specific thermal plamsa configuration, one needs to calculate the ionization process, which determines the birth location of the fast ions, and the fast ions orbit to determine whether the trajectories touch the wall. This paper reports the results of this kind of calculations, which are performed for the Experimental Advanced Superconducting Tokamak (EAST) located in Hefei and managed by Institute of Plasma Physics, Chinese Academy of Sciences. One property of EAST relevant to neutral beam injection is that EAST is equiped with coils that can produce three-dimensional (3D) magnetic perturbations, which are often called Resonant Magnetic Perturbation (RMP) and are designed for the control of Edgy Localized Modes (ELMs)[?], but turns out to also have effects on the prompt loss of neutral beam fast ions. These effects are modeled by a newly developed Monte-Carlo code that calculates the ionization and the prompt loss under the influence of the 3D magnetic perturbations produced by the RMP coils.

The remainder of this paper is organized as follows. Section 2 describle the model used in modeling the neutral beam source (the part that is outside the tokamak vacuum). Section 3 describles the method of computing the ionization process and the initial spatial distributions of the fast ions generated, which are compared with the results obtaind from an established NBI modeling code, NUBEAM[?]. Section () discusses the prompt loss of fast ions under the influence of the RMP coils, where the spatial distribution of the lost ions on the first wall is given. A brief summary is given in Sec. ().

a paragraph discussing something new found in this work.

## 2 Neutral beam source

To create beam of neutral particles of high energy for the purpose of heating tokamak plasma, one usually needs a system consisting of (1) an ion source, which produces low-energy ions, (2) a set of accelerating grids, which is attached to the window of the ion-source arc-chamber, to accelerate the

ions to energetic ion beam, (3) a neutralizing chamber, which neutralizes the ion beam to neutral beam, and (4) a bending magnet to remove remained charged particles from the beam. Figure 1 shows a sketch map of the accelerating grids of EAST neutral beam system.

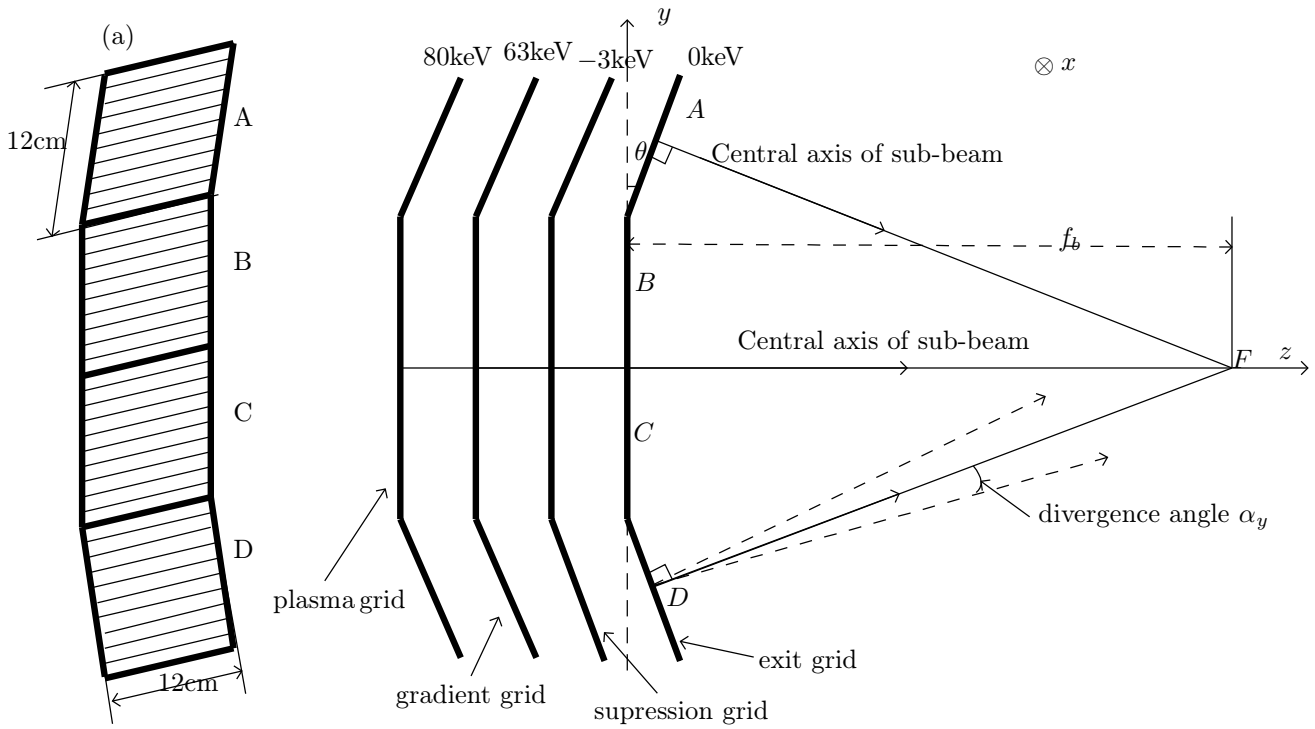


**Figure 1.** (a) Three-dimenional sketch map of one of the accelerating grids. (b) Sketch map of the side vew of the four groups of accelerating grids of EAST neutral beam injector, which are called plasma grid, gradient grid, suppression grid, and exit grid, respectively. Each accelerating grid has four sub-grids, indicated by $A$, $B$, $C$, and $D$ on the figure. Sub-grids $A$ and $D$ are rotated with respect to the centeral sub-grids $B$ and $C$ by a small angle $\theta = \left(1\frac{1}{12}\right)^\circ$. This angle is exaggerated on the figure. The central axis of the two sub-beams (beams from sub-grid $A$ and $D$) intersect at F. The vertical focal length $f_b$ is defined as the distance from point $F$ to the plane of $BC$ grids. Each sub-grid is a 12cm × 12cm square. A typical setting of the voltage on the grids is indicated on the figure.

The geometrical shaping of the accelerating grids is one of the factors that determine the properties of the beams emitting from the grids. One property related to the shaping is the focal length of the beam. Neglecting the beam divergence (discussed later), the central beam from each sub-electrode is perpendicular to the corresponding grid plane. As is shown in Fig. 1, two of the sub-electrodes $A$ and $D$ are rotated to the right with respect to the centeral sub-electordes by a small angle $\theta$. This focuses the central beams from $A$ and $D$ with a focal length given by

$$f_b \approx \frac{L_y}{\tan(2\theta/3)}, \tag{1}$$

where $L_y$ is the vertical length of the sub-grid. For EAST neutral beam system, $\theta = \left(1\frac{1}{12}\right)^\circ$ and $L_y = 0.12m$, Eq. (1) gives that the focal length $f_b \approx 9.52m$. This is the focus length on the vertical plane ($(y,z)$ plane). The horizontal focal length (on $(x,z)$ plane) is infinity for EAST NBI because all the sub-electrodes are flat in the horizontal direction.

Another important property of a beam is the beam divergence. The direction of velocity of ions emitting from the exit grid usually deviates from the central axis of the beam. This deviation is called beam divergence (see Fig. 1). In Monte-Carlo method used in this work, the beam divergence is implemented by setting the veolocity direction (via setting $\alpha_y$ and $\alpha_x$ defined below) of the loaded markers on the exit grid plane according to the following Gaussian distributions:

$$P(\alpha_y) = \frac{1}{\sqrt{2\pi}\alpha_{y0}} \exp\left(-\frac{\alpha_y^2}{2\alpha_{y0}^2}\right), \tag{2}$$

and

$$P(\alpha_x) = \frac{1}{\sqrt{2\pi}\alpha_{x0}} \exp\left(-\frac{\alpha_x^2}{2\alpha_{x0}^2}\right), \tag{3}$$

where $\alpha_y$ is the angle between the beam central axis and the projection of the particle velocity on $(y, z)$ plane, as is shown in Fig. 1, and similarly $\alpha_x$ is the angle between $\hat{\mathbf{z}}$ and the projection of the velocity on $(x, z)$ plane, $\alpha_{x0}$ and $\alpha_{y0}$ are the standard deviations of the distributions, which in this case characterize the magnitude of the beam divergence. After loading particles according to the above distribution, each particle gets specific values of $\alpha_x$ and $\alpha_y$, which determines the actual velocity direction of each particle. Sepcificly, the angle $\alpha_2$ between $\hat{\mathbf{z}}$ and the projection of the particle velocity on $(y, z)$ plane (see Fig. 2) is given by $\alpha_2 = \theta_0 + \alpha_y$, where $\theta_0 = \theta$ for markers emitting from the grid $D$, $\theta_0 = -\theta$ for markers emerging from the grid $A$, $\theta_0 = 0$ for markers emitting from the grids $B$ and $C$. Similarly, the angle $\alpha_1$ between $\hat{\mathbf{z}}$ and the projection of particle velocity on $(x, z)$ plane (see Fig. 2) is given by $\alpha_1 = 0 + \alpha_x$, since the projection of beam axis on $(x, z)$ plane is parallel to $\hat{\mathbf{z}}$ axis.

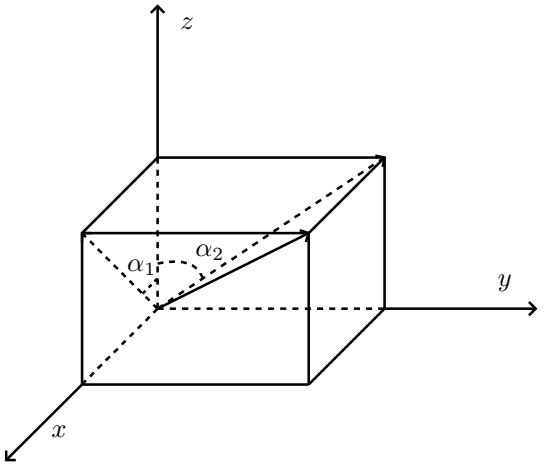


**Figure 2.** Direction of the particle velocity is determined by $\alpha_1$ and $\alpha_2$, where $\alpha_1$ is the angle between $\hat{\mathbf{z}}$ and the projection of the particle velocity on $(x, z)$ plane, and $\alpha_2$ is the angle between $\hat{\mathbf{z}}$ and the projection of the velocity on $(y, z)$ plane.

The focus and divergence of the beams, although small, have significant effects on the beam entering in the plasma because there is a long distance from the accelerator to the torus (about $9m$ for EAST).

The above discussion adresses the velocity direction of the particles emitting from the accelerating grids. Besides the direction, we need to set the magnitude of the particle velocity (or the kinetic energy). For the EAST neutral beam system, which uses Deuteron ion-sources, a particle going through the accelerating grids can be a Deuteron (denoted by $D^+$), or a Deuteron combined with one or two additional Deuterium atoms (denoted by $D_2^+$ and $D_3^+$). The number ratio between $D^+$, $D_2^+$, and $D_3^+$ entering the acelerating grids is determined by the ion-source. All particles ($D^+$, $D_2^+$, and $D_3^+$) going through the accelerating grids get the same kinetice energy $eU$ because they are all single-charged and passing through the same voltage drop, where $e$ being the elementary charge and $U$ the voltage drop on the accelerating grids. These charged particles then pass through the neutralizing chamber, which neutralizes the ion beam to a neutral beam. The neutralizing efficiency depends on the velocity of the particles. Since the velocity of $D^+$, $D_2^+$, and $D_3^+$ is different from each other, the ratio between the corresponding neutralized single-atom, bi-atom, trip-atom particles (denoted by $D$, $D_2$, and $D_3$, respectively) is changed from the ratio between $D^+$, $D_2^+$, and $D_3^+$ emitting from the acelerating grids. The particle number ratio between $D$, $D_2$ and $D_3$ is estimated to be $80\%: 14\%: 6\%$ for the EAST neutral beam system and this ratio is used as an input to set the neutral beam source. The kinetic energy of $D_2$ and $D_3$ is divided equally by thier components atom when they separate from each other, which generates single-atom particles of kineitc energy $E_{\text{full}}/2$, and $E_{\text{full}}/3$, where $E_{\text{full}} = eU$. In the simulations, all markers loaded are

considered as single-atom particles and thus the particle number ratio between particles with $E_{\text{full}}$, $E_{\text{full}}/2$, and $E_{\text{full}}/3$ are identical to the particle number ratio between $D$, $D_2$ and $D_3$, i.e., 80%: 14%: 6%. In the simulation, kinetic energies of markers are randomly chosen among the three energies while satisfying the above number ratio between them.

The neutralizing process is not directly modeled in the simulation and its effect is included only through the input number ratio between particles with energies of $E_{\text{full}}$, $E_{\text{full}}/2$, and $E_{\text{full}}/3$. We assume that other beam properties (e.g. focus and divergence) are not changed by the neutralizing process, except that only part of the ions succeed in becoming neutrals and the remaining ions will be removed by the deflector magnet before they reach tokamak vacuum.

The spatial distribution of particles on the exit grid is assumed to be uniform and are implemented in the simulation via seting particle location by using a uniformly distributed random variable.

After setting all the above parameters, each marker gets a set of well-defined initial conditions, which can be used to determine its subsequent orbit, which is assumed to be along a straight line until the marker arrives at the ionization location in the plasma. In addition, due to the finite size of the vacuum window, through which neutral particles need to pass to enter the vacuum, those particles with large divergence angles can not pass through the window to enter the vacuum and this effect is modeled in the simulation.

## 3 Monte-Carlo implementation of birth of fast ions due to ionization of neutral beams in plasma

When a neutral beam go through plasmas, along the trajectory of the beam, the beam intensity is attenuated due to the ionization of neutral particles by the background plasma. The attenuation of beam intensity can be modeled by the following differential equation:

$$\frac{dI}{dl} = -\nu(l) I, \tag{4}$$

where $I(l) = n_b(l) v_b$ is the beam intensity, $n_b$ is the number of beam particles per unit length along the beam trajectory and $v_b$ the beam velocity (assumed to be constant along the trajectory), and $\nu(l)$ is given by

$$\nu(l) = n_i \sigma_{\text{ch}} + n_i \sigma_i + n_e \frac{\langle \sigma_e v_e \rangle}{v_b}, \tag{5}$$

where $n_i$ and $n_e$ are the number density of background plasma ions and electrons, respectively, $\sigma_{\text{ch}}$ is the cross-section for charge exchange with plasma ions, $\sigma_i$ are the cross-section for ionization by plasma ions, $\langle \sigma_e v_e \rangle$ is the electron impact ionization rate coefficient averaged over the Maxwellian distribution ($\langle \sigma_e v_e \rangle / v_b$ is the effective cross-section of electron impact ionization). The ionization cross-sections data used in this work are provided in Apendix ().

The solution to Eq. (4) can be analytically obtained, which is given by

$$I = I_0 e^{-\int_0^l \nu(l') dl'}, \tag{6}$$

where $I_0$ is the beam density at the starting point of the beam trajectory. The solution (6) indicates an exponential attenuation of the beam intensity along the beam trajectory.

The Monte-Carlo method of implementing the beam attenuation due to ionization process is as follows. First associate each markers loaded with a uniformly distributed random number $\eta$ in the range of [0, 1]. Then, along the trajectory of each neutral particle (straight line), the integration $s = \int_0^l \nu(l') dl'$ is calculated to examine whether $s \geqslant \ln(1/\eta)$ or not. If $s \geqslant \ln(1/\eta)$, then the neutral particle is considered to be ionized. A simple numerical experiment can verify that this implementation generate results in agreement with the analytic solution given by Eq. (6). However, the Monte-Carlo implementation provides more details on the process besides the beam intensity, namely the ionization locations of each markers loaded in the simulation, and this locations are ready to be used in the sebquent orbit following computations of this work. Those neutral particles that are not yet ionized when they reach the inner wall of the device are usually lost to the wall and this loss of neutral particles are called shine-through loss, which is discussed in Sec. ().

## 3.1 Benchmarking the new code with NUBEAM code

To verify the reliability of the new code in modeling the ionization process, we carried out a benchmarking case with the NUBEAM code[?]. The plasma density and temperature profiles used in the benchmarking case are shown in Fig. 3.

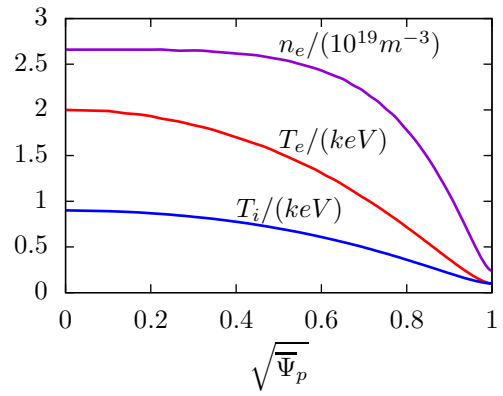


**Figure 3.** Profiles of electron number density , electron temperature, and ion temperature used in the benchmarking case, where the radial coordinate, $\sqrt{\overline{\Psi}_p}$ , is the square root of the normalized poloidal magnetic flux. These profiles are for EAST discharge #59954@3.0s.

The ionization cross-sections used in the new code, which is given in Apend. (), do not include the contributions from multi-step ionization process. Multi-step ionization refers to the case where a collision push a neutral into its excited state and a subsequent collision revmove the electron from the neutral before the elecron decays to its ground state. NUBEAM include the excited state correction due to this multi-step ionization and this correction is turned off in the benchmarking case. Furthermore, the ionization due to collsion with impurities is not included in the new code and is turned off in NUBEAM in the benchmarking case. The comparison of the beam density deposition profiles calculated by the new code and NUBEAM code are shown in Fig. 4.

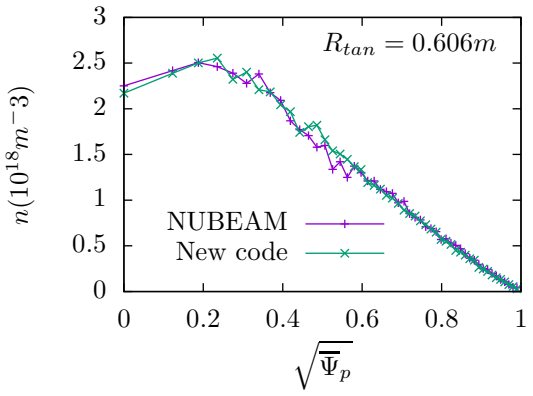


**Figure 4.** Comparision of flux-surface averaged densities of ionized neutrals calculated by NUBEAM and the new code of this work.

## 3.2 Two-dimensional distribution of fast ions

Figure 5a gives the two-dimensional distribution of ionized particles on the poloidal plane (averaged over the toroidal direction). Figure 5b gives the top view of the distribution of ionized particles (averaged over the vertical direction). The results indicate that most fast ions are born at the low-field-side.

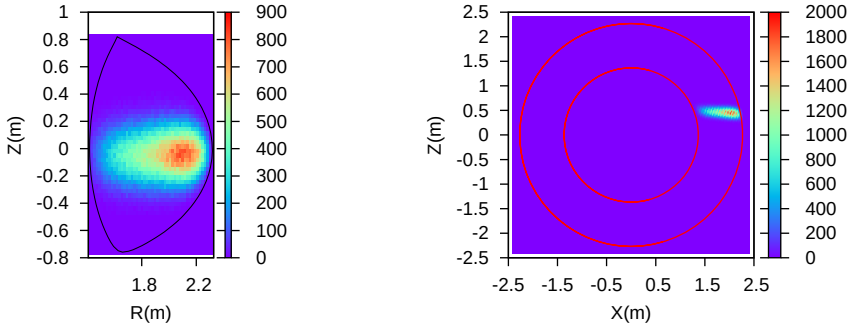


**Figure 5.** Rtan=0.606m, left: poloidal view, right: top view

# 4 RMP coils on EAST tokamak and thier effect on magnetic field toponology

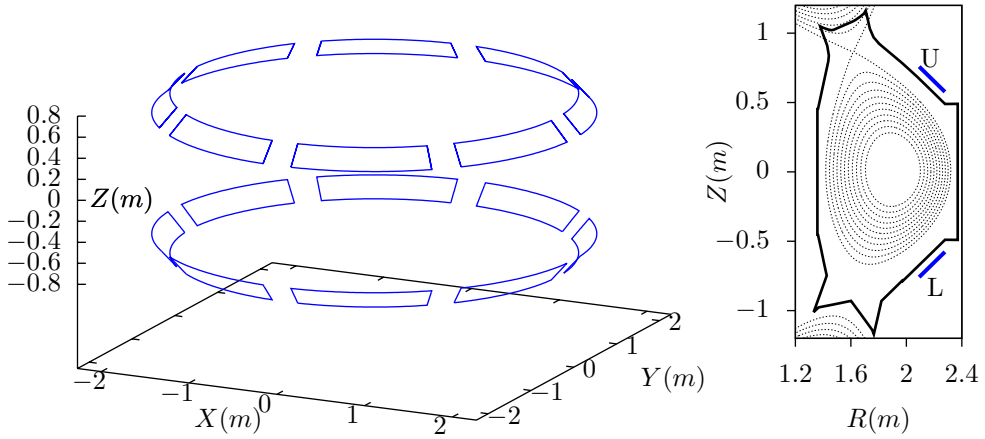


**Figure 6.** Location of the RMP coils on EAST tokamak in 3D view (left) and poloidal view (right).

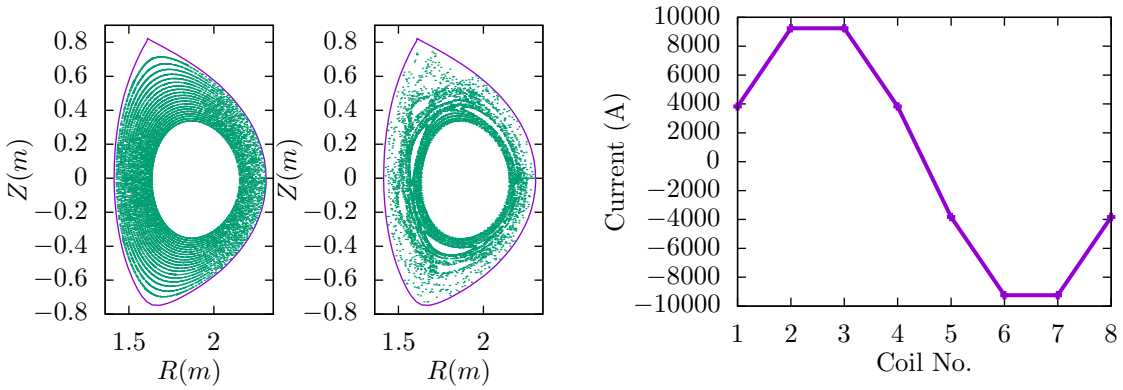


**Figure 7.** Poincare section of magnetic field lines of axisymmetric magnetic field (left) and the superpostion of the axisymmetric magnetic field and a magnetic perturbation generated by RMP coils (middle). Right: current in each RMP coil. The axisymmetric magnetic field is from EAST discharge #59954@3.1s. These Poincare sections are obtained by tracing 20 field lines starting from 20 points on the the low-field-side midplane, and then then recording the intersecting points of these field lines with the $\phi = 0$ plane. The maximum number of intersecting points for each field line is set to 700. In (a), i.e. axisymetrica field, the Poincare points form nested surface, which inidcates the accuracy of the field line tracing is good. In (b), some field lines touch the first wall of the machine before they finish 700 toroidal turns.

# 5 Prompt loss under the influence of RMP

For the shine-through loss to be small, most neutral must ionize at the low-field-side (most neutrals ionizing at the the high-field side usually means a very high shine-through loss fraction). As is well known, an ion born at the low-field side with a counter-current initial velocity has an orbit that is outside of the magnetic surface where it is born. Therefore this kind of ions are more likely to touch the wall and thus to be lost (an example is given in Fig. 8), which implies that counter-current neutral beam injection usually suffers larger prompt loss than the co-current injection.

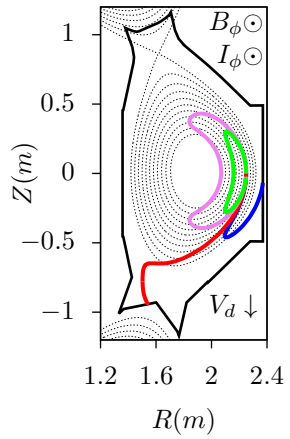


**Figure 8.** Poloidal orbits of Deuterium particles of 50keV ionized at the low-field-side midplane ($R=2.25m$, $Z=0m$) with a birth pitch angle $\theta=125°$ (red), $\theta=105°$ (blue), $\theta=75°$ (green), and $\theta=65°$ (violet). Pitch angle $\theta$ is the included angle between the magnetic field and the velocity of particles. Since the magnetic field and the plasma current are in the same direction for this case, $\theta>90°$ means counter-current injection and $\theta<90°$ means co-current injection. The counter-injected particles are easy to be lost from the plasma because their orbits are outside the flux surface where they are ionized, and thus are more likely to touch the first wall.

Using the initial distribution of fast ions calculated by the neutral deposition code, the guiding-center orbit of each fast ion is followed to check whether it touchs the wall. Those touching the wall are considered lost. Figure ()-() compare the time evolution of the loss fraction of fast ions in the cases with RMP and those without RMP.

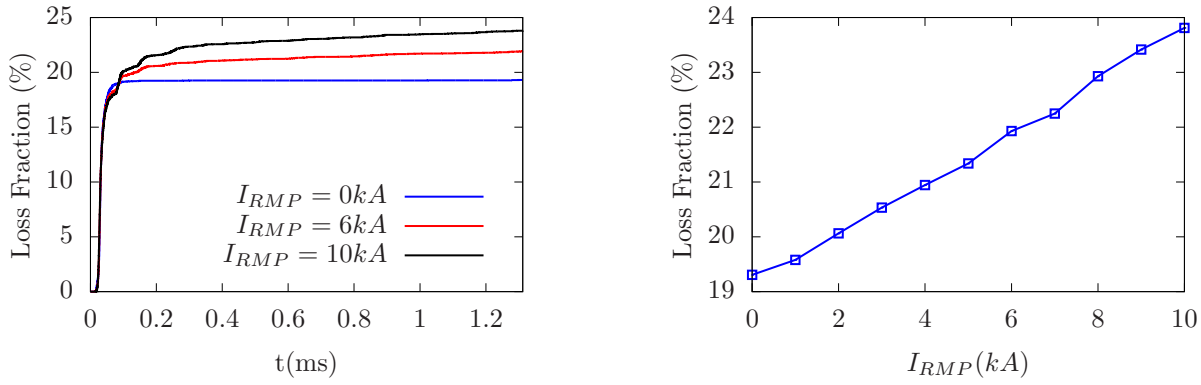


**Figure 9.** RMP with $n=1$ and up-down symmetry, counter-current injection, Rtan=0.606m, Equilibrium file: g059954.003030

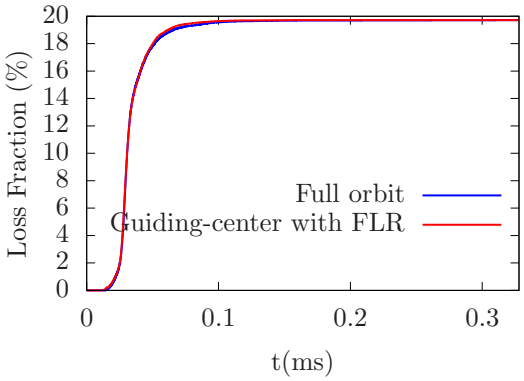


**Figure 10.** comparison between results obtained by full orbit model and guiding-center model, counter-current injection, Rtan=0.606m, Equilibrium file: g059954.003030

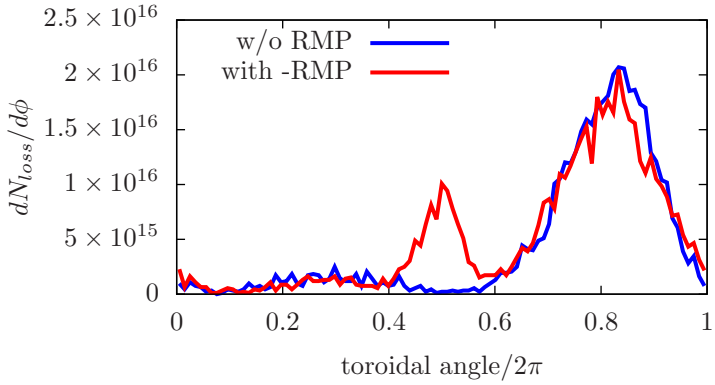


**Figure 11.** Rtan=0.606, cntr-Ip , in EAST discharge #59954@3.2s

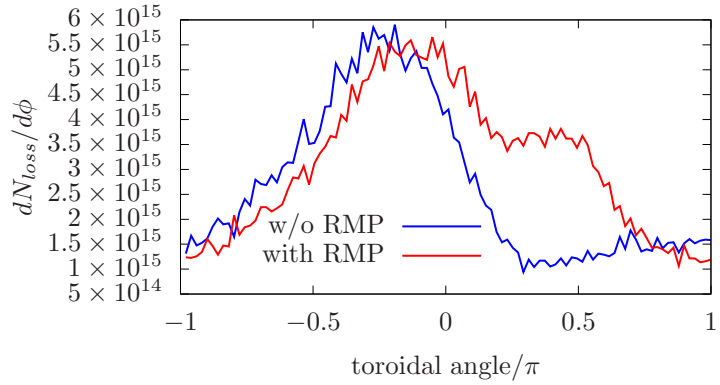


**Figure 12.** Rtan=0.606, cntr-Ip , in EAST discharge g059954.003030

# 6 Summary

# 7 ACKNOWLEDGMENTS

One of the authors (Y. Hu) acknowledges useful discussions with Youwen Sun, Bin Wu, Jinfang Wang, Wei Chen, and Wei Shen. Numerical computations were performed on the ShenMa High Performance Computing Cluster in Institute of Plasma Physics, Chinese Academy of Sciences. This work was supported by the National Magnetic Confinement Fusion Science Program of China under Grant No. 2013GB112010 and the National Natural Science Foundation of China under Grant No. 11575251.

# Appendix A Ionization cross sections of neutral particles in plasmas

The three ionization cross-sections mentioned in Sec., namely, cross-section for charge exchange with plasma ions $\sigma_{\rm ch}$, cross-section for ionization by plasma ions $\sigma_i$ , and the effective cross-section of electron impact ionization $\langle \sigma_e v_e \rangle / v_b$, depends on the beam velocity $v_b$. The effective cross-section of electron impact ionization is special in that it also depends on the temperature of background electrons.

The cross-section for charge exchange with plasma ions $\sigma_{\rm ch}$ is plotted in Fig. 13 as a function of the kinetic energy per amu (atom mass unit).

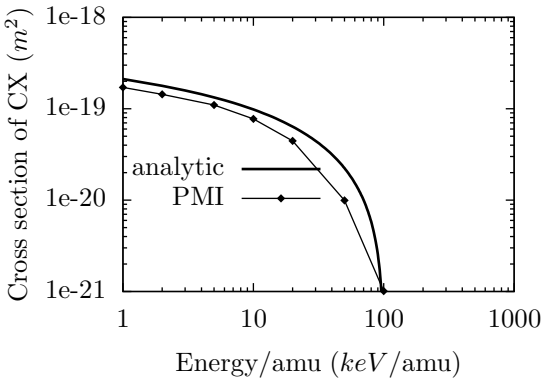


**Figure 13.** Cross section of charge exchange between Hydrogen-Hydrogen (including the isotopes $^1H$, $^2H$, and $^3H$) as a function of the kinetic energy per amu (atom mass unit). The results labeled by "PMI" is from the data on Page 78 of Ref. [2]. The analytic fitting results (black line) are from Eq. (28) of Ref. [1], which is given by $\sigma_{ex}(m^2) = 10^{-18}(1 - 0.5(2E)^{0.06} + 4 \times 10^{-7}E)$, where $E$ is the collision energy per amu in eV/amu. The values of the fitting cross section agrees with those given in Fig. 5.3.1 of Wesson's book[?].

Kaganovich's paper[3] gives the following fitting formula for the impaction ionization cross section by a fully stripped ion, $\sigma_i$:

$$\sigma_i(v, I_{\rm nl}, Z_p) = \pi a_0^2 \frac{N_{\rm nl} Z_p^2}{(Z_p+1)} \frac{E_0^2}{I_{\rm nl}^2} G^{\rm new}\left(\frac{v}{v_{\rm nl}\sqrt{Z_p+1}}\right), \tag{7}$$

where $v$ is the relative velocity between the atom and the ion, $Z_p$ is the atomic number of the fully stripped ion, $I_{\rm nl}$ is the ionization potential of the atom, $v_{\rm nl} = v_0\sqrt{2I_{\rm nl}/E_0}$ with $v_0 = 2.2\times10^6 m/s$ and $E_0 = 27.2$eV, $N_{\rm nl}$ is the number of electrons in the $nl$ orbital of the atom ($N_{\rm nl}=1$ for hydrogen), $a_0 = 0.529\times10^{-10} m$ is the Bohr radius, and $G^{\rm new} = x^{-2}\exp(-x^{-2})[1.26+0.283\ln(2x^2+25)]$.

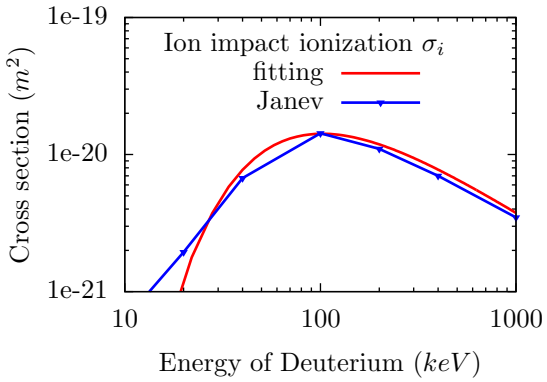


**Figure 14.** Cross section of ion impact ionization of deuterium as a function of the kinetic energy of deuterium atom (red line is calculated by using Eq. (7), data of blue line are from the data on Page 68 of Ref. [2]).

For neutral beam injection relevant to present tokamaks, the thermal velocity of plasma ions are much smaller than the velocity of beam atoms, i.e., $v_{ti} \ll v_b$, so that $v_{ti} \approx 0$ can be assumed. As a result, $\sigma_{\rm ch}$ and $\sigma_i$ discussed above are independent of the temperature of the background plasma ions. However, the electron impact ionization rate coefficient $\langle\sigma_e v_e\rangle$ usually depends on the temperature of background electrons because the thermal velocity of electrons is usually comparable to the beam velocity and an averaging over the electron Maxwellian distribution is needed. The dependence of the electron ionization rate coefficient $\langle\sigma_e v_e\rangle$ on the electron temperature is plotted in Fig. 15.

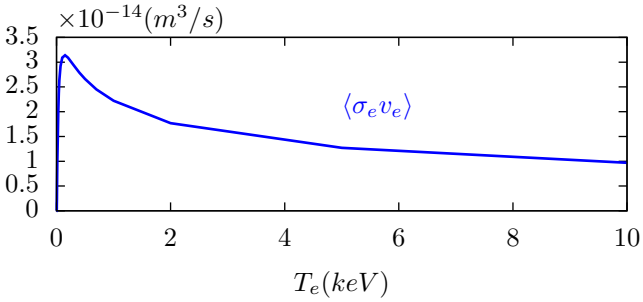


**Figure 15.** The dependence of the electron impact ionization rate coefficient $\langle\sigma_e v_e\rangle$ on the electron temperature $T_e$. These data are obtained by using the open-ADAS reading program "xxdata_07" to acces the ADAS data file "szd93#h_h0.dat", which stores the electron ionization rate coefficient for hydrogen atom.

Knowing $\langle\sigma_e v_e\rangle$, the electron impact ionization cross section is given by $\langle\sigma_e v_e\rangle / v_b$, where $v_b$ the velocity of beam particles. Fig. 16 plots the dependence of the electron impact ionization cross section on the kinetic energy of Deuterium atom for different backgound electron temperatures.

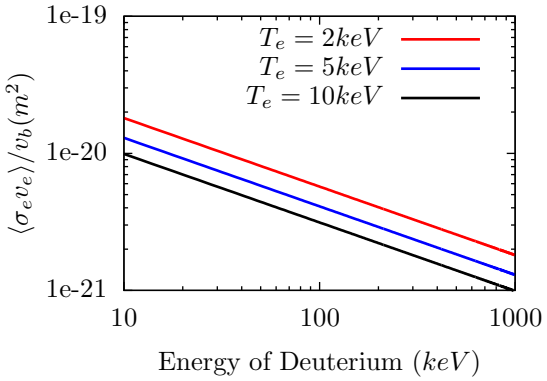


**Figure 16.** The dependence of the electron impact ionization cross section $\langle \sigma_e v_e \rangle / v_b$ on the kinetic energy of Deuterium atom for the three cases with $T_e = 2$keV, 5keV, and 10keV.

In this work, the analytical fitting formula for the cross-sections are not used in the simulations. The simulations directly use numerical spline interpolation to obtain the values of the cross-sections from the data provided in Janev's paper[?] and the ADAS database[?].

—

In Monte-Carlo simulations, to represent the particles source emitting from the accelerating grids, an assemble of markers are loaded with desired distribution over space, energy and direction of velocity.

—

# Bibliography

**[1]** O. Demokan and V. Mirnov. Rigorous treatment of charge exchange, ionization, and collisional processes in neutral-beam-injected mirrors. *Physics of Plasmas*, 2(1):139–145, 1995.

**[2]** R. K. Janev and J. J. Smith. Cross sections for collision processes of hydrogen atoms with electrons, protons and multiply charged ions. *Atomic and Plasma-material Interaction Data for Fusion*, 4, 1993.

**[3]** Igor D. Kaganovich, Edward A. Startsev, and Ronald C. Davidson. Scaling cross sections for ion-atom impact ionization. *Physics of Plasmas*, 11(3):1229–1232, 2004.

**[4]** Charles F. F. Karney. Fokker-planck and quasilinear codes. *Comp. Phys. Rep.*, 4:183–244, 1986.

**[5]** Z. Lin, W. M. Tang, and W. W. Lee. Gyrokinetic particle simulation of neoclassical transport. *Physics of Plasmas*, 2(8):2975, 1995.

**[6]** ITER physics basis editors. Chapter 5: physics of energetic ions. *Nucl. Fusion*, 39(12):2471, 1999.

**[7]** Y. Todo, M.A. Van Zeeland, A. Bierwage, and W.W. Heidbrink. Multi-phase simulation of fast ion profile flattening due to alfvén eigenmodes in a diii-d experiment. *Nucl. Fusion*, 54(10):104012, 2014.